ACS Macro Letters

Letter

pubs.acs.org/macroletters

Microscopic Origin of the Non-Newtonian Viscosity of Semiflexible Polymer Solutions in the Semidilute Regime

Benjamin Huber,[†] Markus Harasim,[†] Bernhard Wunderlich,[†] Martin Kröger,[‡] and Andreas R. Bausch*[,†]

[†]Lehrstuhl für Biophysik, Technische Universität München, D−85748 Garching, Germany

[‡]Department of Materials, Polymer Physics, ETH Zurich, CH−8093 Zurich, Switzerland

ABSTRACT: One of the great goals in polymer physics is to relate the various macroscopic features of polymeric fluids with the microscopic behavior of single chains. Here, we directly visualize the conformational dynamics of individual semiflexible polymers in a semidilute solution above the overlap concentration under shear. We observe that the tumbling dynamics are significantly slowed down, in marked contrast to the case of a dilute solution, due to steric interactions with neighboring filaments. The observed macroscopic shear thinning effect can be rationalized by a simple model based on the single filament dynamics.

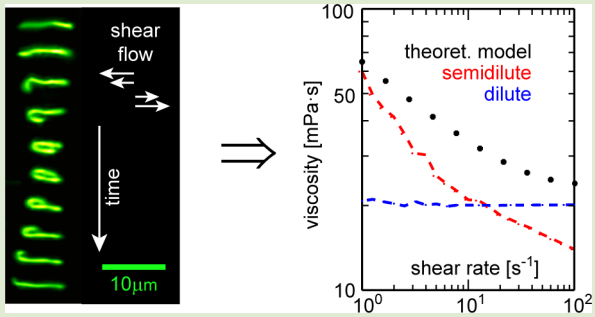

Polymeric liquids show very different rheological behaviors dependent on their polymer/solvent ratio: In the dilute regime, only solvent−solvent and polymer−solvent interactions contribute to rheology and the solution behaves similar to a pure solvent. Above the overlap concentration, interactions between the polymers dominate the behavior of the fluid and it becomes viscoelastic. The viscoelasticity increases with increasing polymer concentration and reaches its maximum within a melt. The individual configurational dynamics of polymers in dilute solutions under shear have already been elucidated. Single filament responses to interactions with the solvent, such as stretching and tumbling, have been identified both in experiments and in simulations.[1−8] A recently introduced microscopic setup based on a semiautomated moving stage allowed the introduction of a quantitative telescopic Brownian rod model, which fully accounts for the individual filament dynamics in such a dilute regime.[4] Yet how the presence of polymers in the overlap regime influences the dynamics of single filaments and how this in turn couples back to the macroscopic flow behavior and viscosity remains unresolved. Especially, relating the non-Newtonian flow behavior of polymer solutions above the overlap concentration to the microscopic dynamics of individual filaments has proven to be difficult, mostly due to the lack of experimental insights into the microscopic dynamics of the individual constituents.

Here, we directly visualize the configurational dynamics of individual semiflexible polymers in the semidilute regime under shear flow conditions (Figure 1). In this concentration regime, the solution exhibits a shear thinning behavior. We present a minimal model relating the microscopic behavior of single chains to the macroscopic viscosity of the polymer solution. Mixtures of labeled and unlabeled actin filaments above the overlap concentration flow through microfluidic channels on a semiautomatic moving stage. The configurational dynamics of individual filaments are observed using fluorescence microscopy. We identify that the major effect of the entanglement on the filament dynamics is the prolonged time filaments spend in the extended configuration. Compared to the dilute regime, tumbling events occur less often, yet the time the filament ends need to reverse the direction is the same. In addition, anomalous and aborted tumbling events occur (Figures 1b−d). The determined angular probability distribution can directly be used to recover the macroscopic viscosity because the stress tensor including its shear component can be expressed, within the framework of nonequilibrium thermodynamics,[9−11] in terms of anisotropic moments of the distribution function. Such moments, also known as orientation tensors, fully characterize the amount of flow-induced alignment of the assumed uniaxial particles.

To visualize the single polymer dynamics in the semidilute regime, a small amount of filaments which are fluorescently labeled with AlexaFlour488-phalloidin is added to a 10 μM solution of unlabeled actin. Actin is polydisperse with a monoexponentially decreasing length distribution with a decay length of 4.3 μm. A dilute reference solution consists of labeled polymers (0.5 nM) and glycerol to match the viscosity of both solutions at the observed shear rate. The polymeric liquids are pumped through Polydimethylsiloxane (PDMS) microchannels and the motion of single filaments is recorded with a CCD camera using a semiautomated moving stage.[4] As proposed in ref 11, we evaluate the angle ϕ between the filaments' end-to-end-vectors and the flow direction of filaments with comparable contour lengths of $L_c \approx 8$ μm and subjected to a shear rate $\dot{\gamma} \approx 10$ s^{-1} to statistically quantify the behavior of the polymers (Figure 1).

Received: November 25, 2013
Accepted: January 7, 2014
Published: January 14, 2014

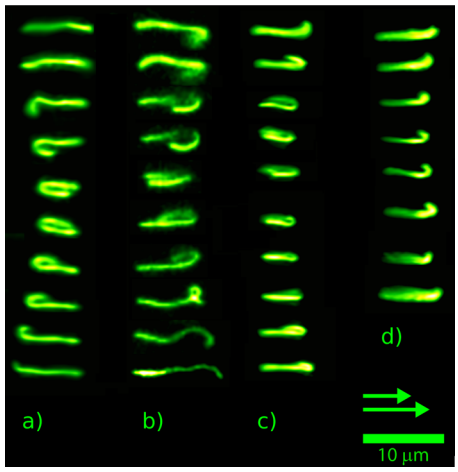

Figure 1. From top to bottom: Successive images of four filaments in a semidilute solution subjected to shear flow. The contour lengths of the filaments are (a) L_c = 9.0, (b) 11.5, (c) 8.2, and (d) 8.1 μm and the shear rates are (a) $\dot{\gamma}$ = 10.9, (b) 4.3, (c) 8.0, and (d) 12.0 s^{-1}. The time between two subsequent images is (a) 242, (b) 2046, (c) 428, and (d) 186 ms. Due to the applied velocity gradient, shown schematically with green arrows at the bottom right, the filament's ends overtake each other. Normally, a chain's end located in the region with faster fluid velocity moves to the front, as can be seen in (a). In a semidilute solution, we also observe that the end in the slower region overtakes the faster one (b). In addition to these "anomalous" tumblings, some filaments eventually start tumbling, stop, and are then drawn back to their initial orientation. Such aborted tumblings are shown in (c) and (d). These two phenomena must be due to interactions with other filaments from the bulk (scale bar = 10 μm).

Semiflexible actin filaments show characteristic tumbling behavior in shear flow. Two characteristic time scales can be identified in the observed tumbling motion of the filaments: A diffusive dominated time τ_{diff}, in which the polymer is predominantly in a stretched conformation aligned with the flow, and an advection time τ_{adv}, during which the transport of the filament ends results in an exchange of the polymer's direction. The critical angle ϕ_c separating the diffusive and the advective dominated phases has been found as $\phi_c = (D_r/\dot{\gamma})^{1/3}$ in dilute solution,[4] where D_r is the rotational diffusion coefficient of the filament in the diffusive phase. For the dilute case, the mean tumbling time of 237 recorded tumblings $\tau_t = \tau_{diff} + \tau_{adv}$ is found to be about 4 s for a set of comparable filaments, with $L_c \approx 8$ μm at $\dot{\gamma} \approx 10$ s^{-1}. The rotational diffusion of the filaments can result in a configuration where bending forces from the shear flow act on a filament end. Only motions with the rotational direction of the shear flow lead to a deterministic motion of the filament ends, resulting in the reversal of the filament orientation. Thus, only two configurational motions are possible: either the front end is turned back in the slower moving shear plane or the rear end overtakes the filament by the transport in the faster shear plane. The whole advective phase is characterized by the U-turn configuration of the filament, set by its bending modulus.[4]

In the semidilute regime, filament−filament interactions lead to an increased tumbling time (Figure 2a). Moreover, we observe aborted tumbling events (Figure 1c,d) where filaments enter the advective phase, yet stop, and are turned back to their initial orientation. Such events are observed in 12% of all observed tumblings in the semidilute regime (196 counted events), where an inclination of a filament end more than 90° away from flow direction was used as a threshold for entering the advective phase. Additionally, we observe tumblings contradictory to the direction conditioned by the velocity gradient, i.e. the end in the slower fluid region overtakes the other (Figure 1b). As both the aborted and the "anomalous" tumblings only occur in semidilute polymeric solutions, while absent in the dilute regime,[4] they must be due to filament−filament interactions. By entanglement forces from different shear planes are readily transferred to a tumbling filament and can directly lead to a reverse direction of the motion in the advective phase. While the aborted tumbling can be readily rationalized by a two-polymer interaction (Figure 3), a complete reverse tumbling can only be mediated by multiple polymer interactions.

To quantify the effects of these interactions on the dynamics, we compared the times spent in the advective and diffusive phase in the semidilute and in the dilute reference solution. As the critical angle ϕ_c represents the point where the rotational diffusion of the filament is equally strong as the advective drift,[4] ϕ_c sets no distinct border to experimentally evaluate the advective and diffusive times. Therefore, we use a threshold angle for the orientation with respect to the flow direction of $25° > \phi_c$ well above the critical angle to evaluate a core "advective time" τ'_{adv} for the disaligned advective phase and a "waiting time" τ_w, including the entire diffusive dominated phase for the flow-aligned phase at lower angles. Figure 2c,d show the distribution of advection and waiting times for the dilute reference solution (blue, 36 tumblings) and the semidilute solution (red, 37 tumblings). Hereby, anomalous tumblings have not been evaluated; aborted tumblings were evaluated as prolonged waiting time. For the conditions studied here, anomalous tumblings occurred only in 3% of all observed events and do not significantly alter the observed characteristics of advective and waiting times in the semidilute case.

The distribution of the observed advection times is almost identical for both the dilute and the semidilute regime (Figure 2d), so that the advective phase is not significantly affected by the presence of the surrounding filaments unless an anomalous or interrupted tumbling is induced. Yet the distribution of the waiting times is significantly broadened and the average waiting time is shifted by a factor of 2 (Figure 2c). The prolonged diffusive times are due to the high density of surrounding filaments, which presumably prevent the filaments to enter the advective phase by steric hindrance. In addition, the aborted tumblings contribute directly to the prolonged waiting times.

The prolonged waiting time due to the steric hindrance of the surrounding filaments expresses itself best in the slimmer angular distribution of the orientational vector for the semidilute solution (Figure 2b). Consistent to other literature[10,12] where a 10× higher rotational relaxation time for semidilute DNA compared to the dilute case was reported, we describe this effect with an effective lower rotational diffusion coefficient. The large variation in the waiting time distribution in the semidilute solution can be attributed to the complex dynamics induced by the intermolecular interactions.

Based on the microscopically determined orientational distribution, we propose a simple model with which we compute directly the viscosity of our polymeric solution from the recorded single filament dynamics. This is especially challenging because actin is polydisperse with an exponentially decreasing length distribution. As a starting point, we take the measured probability distribution of the orientational angle of recorded semidilute filaments with a mean length of $L_c^* = 8$ μm and mean shear rate of $\dot{\gamma} = 10$ s^{-1}. The stationary distribution

dx.doi.org/10.1021/mz400607x | ACS Macro Lett. 2014, 3, 136−140

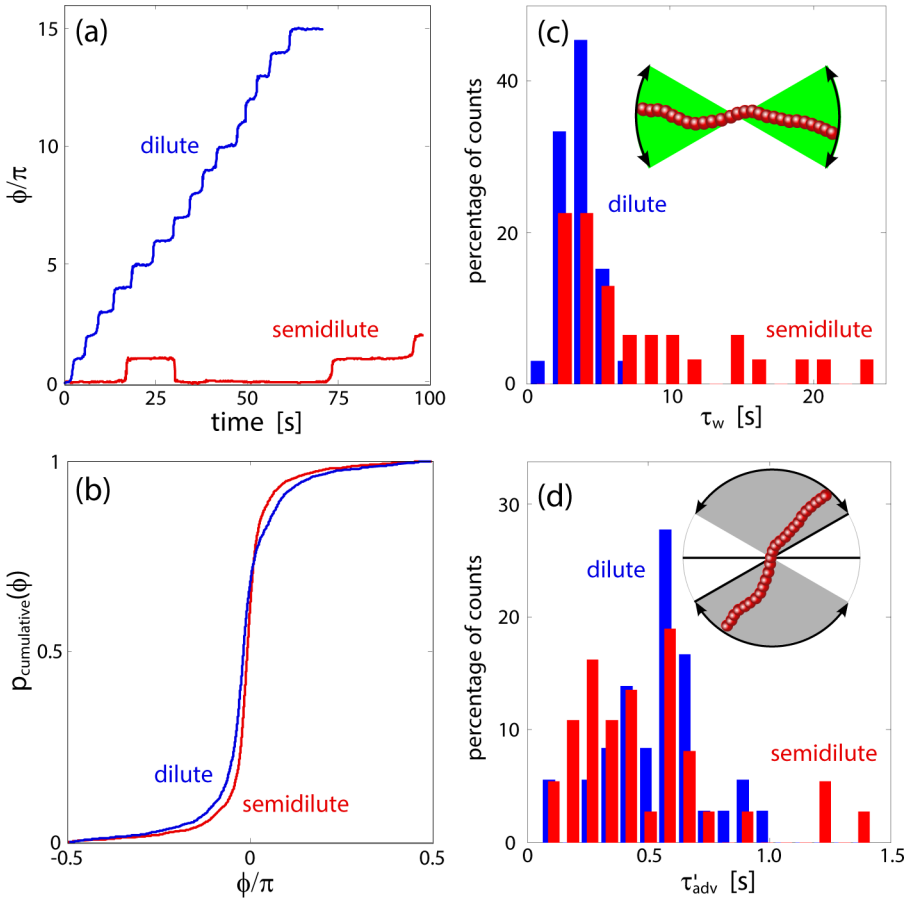

Figure 2. (a) Time course of the orientational angle of the filaments end-to-end vector. The distinct steps show tumbling events whereas the plateaus indicate alignment with the flow. In blue: Filament of length L_c = 8.3 μm in the dilute regime at shear rate 5.0 s^{-1}. In red: Filament with L_c = 9.4 μm in the semidilute regime at shear rate 5.5 s^{-1}. Despite the similar conditions, the dynamics of the filament in the more concentrated regime are significantly slower. The step backward at 30 s shows an anomalous tumbling event. (b) Cumulative distribution for the orientational angle of multiple comparable filaments at shear rate $\dot{\gamma} \approx 10\ s^{-1}$ and contour length $L_c \approx 8\ \mu$m, in the dilute (blue) and semidilute (red) regime. The angular distribution of the semidilute polymers is slimmer and shifted toward the center, consistent with less tumbling and more alignment with the flow. (c, d) Time distributions with comparable lengths and shear rates ($L_c \approx 8\ \mu$m, $\dot{\gamma} \approx 10\ s^{-1}$) in the dilute (blue) and semidilute (red) regime, split at an orientational angle of 25°. Waiting times τ_w (c) for angles lower than 25° with respect to flow direction, advection times τ'_{adv} (d) for higher angles. While the distributions of the advection times appear similar, the waiting times in the semidilute regime have a higher mean value and a much broader variation.

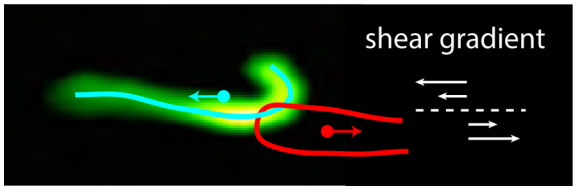

Figure 3. Polymers with their centers of mass in different shear planes can exert forces on each other via entanglements. An aborted tumbling can be caused by an entanglement of two polymers performing their typical U-turn runs in the advective phase. The light blue curve illustrates the contour of a labeled filament (frame taken from the time series in Figure 1d), the red curve represents a possible conformation of an entangled, invisible nonlabeled filament. The arrows indicate the opposing directions of the polymers' center of mass movement.

function contains partial information about the dynamics of the orientation angle. Following ref 4, the temporal evolution of the end-to-end vector $\mathbf{u}$ of a short actin filament subjected to shear is well captured by the one of a Brownian rigid rod, whose deterministic motion is given by $\dot{\mathbf{u}} = (\mathbf{1} - \mathbf{uu}) \cdot \boldsymbol{\kappa} \cdot \mathbf{u}$,[9,10,13] where $\boldsymbol{\kappa} = (\nabla \mathbf{v})^{\dagger}$ denotes the transposed velocity gradient tensor. Introducing polar coordinates, $\mathbf{u} = (\cos \phi, \sin \phi)$, the deterministic part of motion becomes $\dot{\phi}(\phi) = \dot{\gamma}\sin^2(\phi)$ in the case of planar shear. The additional diffusive, or stochastic part of motion is most conveniently captured by formulating a Fokker–Planck (FP) equation for the orientational distribution function $p(\phi)$,

$$\frac{\partial p}{\partial t} = -\frac{\partial(\dot{\phi} p)}{\partial \phi} + D_r \frac{\partial^2 p}{\partial \phi^2} \tag{1}$$

where the orientational diffusion coefficient D_r determines the strength of stochastic contribution. In the absence of flow, the diffusive part is responsible for the relaxation toward equilibrium, where $p(\phi)$ is a constant. In the presence of steady shear flow, eq 1 has a stationary solution, $\partial p_{stat}/\partial t = 0$, that is obtained by first integrating eq 1 over ϕ. The resulting differential equation reads $-D_r^{-1}\dot{\phi} p_{stat} + \mathrm{d}p_{stat}/\mathrm{d}\phi + C = 0$ with an integration constant C that is not needed here but determined by the normalization condition $\int p(\phi)\mathrm{d}\phi = 1$. With the abbreviation $\psi(\alpha) = \exp[D_r^{-1}\int_0^{\alpha} \dot{\phi}\mathrm{d}\phi]$ the stationary FP equation is solved by $p_{stat}(\phi) \sim \psi(\phi)\int_{-\phi}^{\pi-\phi}\psi(\alpha)\mathrm{d}\alpha$, or

dx.doi.org/10.1021/mz400607x | ACS Macro Lett. 2014, 3, 136−140

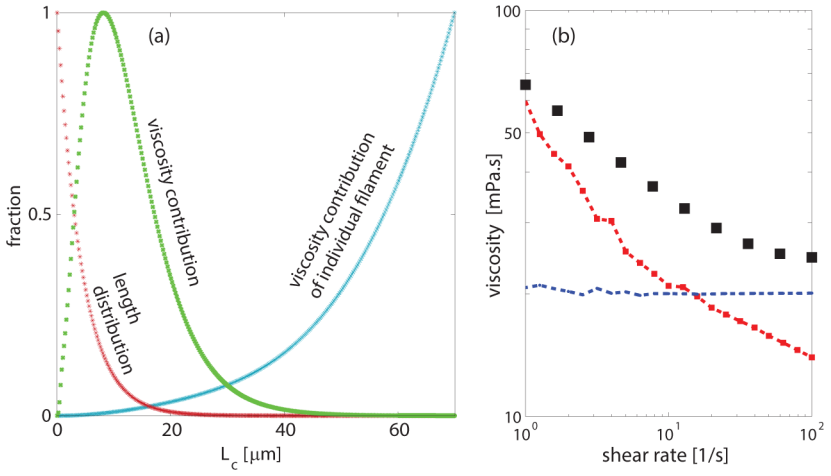

Figure 4. (a) Contribution of single polymers to viscosity increases with increasing contour length (blue). Multiplied with the monoexponential length distribution (red), we obtain the total contribution from all polymers (green) that exhibits a maximum at 8.3 μm. All three curves come with arbitrary units and are scaled to match unity at their maxima. (b) Broken lines show the rheologically measured viscosities of our dilute (blue) and semidilute (red) actin solutions. The background viscosity of the semidilute actin solution is 8 mPas (not shown). The viscosity of the dilute solution was increased by adding glycerol to match with the semidilute one at a shear rate of around 10 s^{-1}. Black squares show the values for the semidilute case, calculated via eq 4 upon using the measured stationary angular distribution, $p_{stat}(\phi)$ in eqs 2 and 3.

equally and numerically more convenient, especially for large $\dot{\gamma}/D_r$ by[14]

$$p_{stat}(\phi) \sim \int_0^{\pi} \exp\left[\frac{\dot{\gamma}}{2D_r}\{\chi - \sin\chi\,\cos(\chi - 2\phi)\}\right]d\chi \quad (2)$$

where χ is an integration variable. We can now directly compare the measured distributions for the dilute and semidilute solutions depicted in Figure 2b with eq 2. The presented approach is motivated by the perception that semiflexible filaments in shear can be described as rods with an effective smaller length.[4] Behind this is the idea that a bendable filament will preferably have an end-to-end-distance below its contour length and will thus show faster dynamics than a rod with the same length. As a result of the comparison, we obtain an effective diffusion coefficient $D_r^* \equiv D_r(L_c^*)$ for the filaments in the semidilute regime which is about four times lower than in the dilute reference solution with the same viscosity. Employing a known[4] approximate expression for $D_r(L_c)$ for semiflexible chains, $D_r(L_c) \sim D_{rod}(L_c/R_{eq})^2$, where $D_{rod} \sim L_c^{-3}$ is the orientational diffusion coefficient of an infinitely thin rod and thus insensitive to the flexibility of the filament, and R_{eq} an effective equilibrium extension of the semiflexible chain, we can eliminate the prefactors and calculate the effective diffusion coefficient for arbitrary lengths via

$$D_r(L_c) = D_r^* \times \frac{L_c^*}{L_c}\left(\frac{R_{eq}(L_c^*)}{R_{eq}(L_c)}\right)^2 \quad (3)$$

Here, $R_{eq}^2 \equiv 1/2[(R_{ee}^{eq})^2 + 12S_{eq}^2]$, involving the equilibrium end-to-end distance R_{ee}^{eq} and gyration radius S_{eq} of the semiflexible chain, is known analytically[13,15] in terms of L_c and the persistence length of an actin filament, $L_p \approx 16$ μm.[4] Although this relation holds strictly true only for the dilute case, it turns out that all L_c-dependent corrections suggested for semidilute regimes[10,16] vanish for a polydisperse case.

With the stationary distribution $p_{stat}(\phi)$ for all L_c at hand and taking into account polydispersity, all moments (orientation tensors) are readily calculated numerically. The contribution of a Brownian rod to the macroscopic stress tensor follows from a Kramers-Kirkwood "virial expression" that is of the form of an average over "force" times "distance".[9,10] For simplicity, we assume that the contribution of a semiflexible filament to the stress tensor is equivalent to that of a Brownian rod with a smaller effective length (eq 3). That is, we employ a stochastic single filament theory where stress and orientation are coupled, and where reverse tumblings could in principle occur only due to thermal motion. Individual collisions with surrounding filaments, that would potentially lead to a positive viscosity contribution, are not captured by such an approach. Accordingly, for the shear component of the stress tensor and the related shear viscosity η, we arrive at

$$\eta = \eta_s + \frac{\nu k_B T}{\dot{\gamma}}\left[-3\langle\cos\phi\,\sin\phi\rangle + \frac{\dot{\gamma}}{2D_r}\langle\cos^2\phi\,\sin^2\phi\rangle\right]$$
$$= \eta_s + \frac{\nu k_B T}{\dot{\gamma}}\int_0^{\infty}\int_{-\pi/2}^{\pi/2}\frac{e^{-L_c/\lambda}}{\lambda}\left[-3\cos\phi\,\sin\phi + \frac{\dot{\gamma}}{2D_r}\cos^2\phi\,\sin^2\phi\right]p_{stat}(\phi)d\phi dL_c \quad (4)$$

where ν and η_s denote the actin concentration and solvent viscosity, respectively, and where the normalized weight $\lambda^{-1}\exp(-L_c/\lambda)$ takes into account the exponentially decreasing length distribution with decay length $\lambda = 4.3$ μm. The concentration of polymers ν we estimate from the concentration of monomers ($c_{mon} = 10$ μM) via $\nu = c_{mon}\delta/\lambda$, where $\delta = 2.77$ nm is the length gain of the filament per monomer. The solvent viscosity is $\eta_s = 8$ mPas at $T = 293$ K. The first contribution in eq 4 is known as stress-optic rule,[9,13] that is, a proportionality between stress and segment orientation tensors that is relevant for the determination of viscoelastic properties of flexible polymers in solutions and melts by means of birefringence measurements,[17] while the second originates from the constraint of constant contour length that comes together with a nonaffine motion of segments. This latter contribution tends to dominate at the large Weissenberg numbers $\sim \dot{\gamma}/2D_r$ under study: the average Weissenberg number Wi for the

dx.doi.org/10.1021/mz400607x | ACS Macro Lett. 2014, 3, 136−140

evaluated $L_c \approx 8$ μm filaments at shear rate $\dot{\gamma} \approx 10$ s^{-1} in the semidilute solution is $Wi = \dot{\gamma}/2D_r^* \approx 1.3 \times 10^3$.

Figure 4 shows how the different lengths contribute to the viscosity of the liquid. The longer an individual filament, the higher its contribution to viscosity. As there are less long filaments than short ones, the total contribution to viscosity by filament length is seen to exhibit a maximum at about 8.3 μm. With these relatively simple assumptions we do not only obtain quite good agreement with the measured viscosity value at the evaluated shear rate, 34.6 mPas compared to 21 mPas via eq 4, but we can also estimate the viscosity at the remaining shear rates (Figure 4b). The occurrence and also the strength of the shear thinning are qualitatively reproduced by the theory and are modeled by the shear rate dependence of p_{stat}, which is due to the increasing flow-alignment of filaments with increasing rate. Note that, by assuming a rigid-rod conformation for the calculation of eq 4, we neglected a second contribution to the shear-thinning: The strongly bent U-turn conformation observed for the semiflexible filaments during the advective motion (Figure 1) further reduces the dissipation between the filament and the solvent. This might explain, why the experimentally determined viscosity in Figure 4b is lower than the theoretical viscosity calculated with a rigid-rod conformation. For concentrations exceeding the semidilute regime, a mean field approach outlined in ref 18 for nonlinear elastic dumbbells could eventually be extended to semiflexible filaments to capture a nonlinear effect of concentration on flow alignment.

In summary, the direct observation of the configurational dynamics of individual filaments in a semidilute polymer solution enabled us to directly relate the orientational distribution to the macroscopic shear thinning behavior. The surprisingly occurring anomalous, collision-induced tumbling events seem to have only a minor effect on the macroscopic flow properties due to their rare occurrence. This contribution may change for more complex fluids or other solvent conditions, where stronger interactions between the constituents occur. Despite its simplicity, the presented model captures surprisingly well the macroscopic behavior and this using only the directly determined parameters, without any free-fit parameters. This is the starting point to also include the effect of the U-turn conformation and thermal bending fluctuations or even more complex dynamics, as observed for flexible polymers. The introduced experimental and theoretical approach sets the basis for a better understanding of complex rheological behavior of ubiquitous polymeric liquids.

AUTHOR INFORMATION

Corresponding Author

*E-mail: abausch@mytum.de.

Notes

The authors declare no competing financial interest.

ACKNOWLEDGMENTS

We thank M. Rusp for the actin preparation. This work was supported by Deutsche Forschungsgemeinschaft through Grant No. BA2029/8 and partly by the Cluster of Excellence Nanosystems Initiative Munich.

REFERENCES

(1) Smith, D. E.; Babcock, H. P.; Chu, S. *Science* **1999**, *283*, 1724−1727.
(2) Teixeira, R. E.; Babcock, H. P.; Shaqfeh, E. S. G.; Chu, S. *Macromolecules* **2005**, *38*, 581.
(3) Steinhauser, D.; Köster, S.; Pfohl, T. *ACS Macro Lett.* **2012**, *1*, 541−545.
(4) Harasim, M.; Wunderlich, B.; Peleg, O.; Kröger, M.; Bausch, A. R. *Phys. Rev. Lett.* **2013**, *110*, 108302.
(5) Hur, J. S.; Shaqfeh, E. S. G.; Larson, R. G. *J. Rheol.* **2000**, *44*, 713−742.
(6) Sendner, C.; Netz, R. R. *Eur. Phys. J. E* **2009**, *30*, 75−81.
(7) Chelakkot, R.; Winkler, R. G.; Gompper, G. *J. Phys.: Condens. Matter* **2011**, *23*, 184117.
(8) Dalal, I. S.; Hoda, N.; Larson, R. G. *J. Rheol.* **2012**, *56*, 305−332.
(9) Bird, R.; Curtiss, C. F.; Armstrong, R. C.; Hassager, O. *Dynamics of Polymeric Liquids*; Wiley: Hoboken, NJ, 1987; Vol. 2.
(10) Doi, M.; Edwards, S. *The Theory of Polymer Dynamics*; Oxford University Press: Oxford, 1986.
(11) Kröger, M. *Phys. Rep.* **2004**, *390*, 453−551.
(12) Teixeira, R. E.; Dambal, A. K.; Richter, D. H.; Shaqfeh, E. S. G.; Chu, S. *Macromolecules* **2007**, *40*, 2461−2476.
(13) Kröger, M. *Models for Polymeric and Anisotropic Liquids*; Springer: Berlin, 2004.
(14) Turitsyn, K. *J. Exp. Theor. Phys.* **2007**, *105*, 655−664.
(15) Rubinstein, M.; Colby, R. *Polymer Physics*; Oxford University Press: Oxford, 2003.
(16) Maeda, T.; Fujime, S. *Macromolecules* **1984**, *17*, 2381−2391.
(17) Fuller, G. G. *Optical Rheometry of Complex Fluids*; Oxford University Press: Oxford, 1995.
(18) Schneggenburger, C.; Kröger, M.; Hess, S. *J. Non-Newtonian Fluid Mech.* **1996**, *62*, 235−251.